Automatic multispectral ultraviolet, visible and near-infrared capturing system for the study of artwork

Jorge Herrera R.*, Meritxell Vilaseca, Jaume Pujol.
Center for Sensors, Instruments and Systems Development, Technical University of Catalonia
Rambla Sant Nebridi 10, Terrassa, Spain.

ABSTRACT

This paper shows the simulations of the usage of a LED cluster as the illumination source for a multispectral imaging system covering the range of wavelengths from 350 to 1650 nm. The system can be described as being composed of two modules determined by the spectral range of the imaging sensors responses, one of them covering the range from 350-950nm (CCD camera) and the other one covering the wavelengths from 900-1650nm (InGaAs camera). A well known method of reflectance estimation, the pseudo-inverse method, jointly with the experimentally measured data of the spectral responses of the cameras and the spectral emission of the LED elements are used for the simulations. The performance of the system for spectral estimation under ideal conditions and realistic noise influence is evaluated through different spectral and colorimetric metrics like the GFC, RMS error and CIEDE2000 color difference formula. The results show that is expectable a rather good performance of the real setup. However, they also reveal a difference in the performances of the modules. The second module has poorer performance due to the less narrow spectral emission and less number of LED elements that covers the near-infrared spectral range.

Keywords: multispectral imaging, LED illumination, simulations, reflectance estimation.

1. INTRODUCTION

Spectral imaging technology has proven its usefulness in a variety of sensing applications ranging from remote sensing, such as satellite or radar imaging, to artwork conservation were it has recently gained importance[1-5]. In the case of the near-infrared region (NIR) the spectral imaging helps in the analysis of paintings identifying pigments through the analysis of the spectra and their distribution over the artwork, besides it provides a good tool in the exploration and study of the underdrawings of the art pieces[6, 7]. In the visible region of the spectra several color related studies, like color imaging and archiving, can also be carried out[8]. Besides, in the case of the UV range, its proper use serves for the detection of organic materials that have fluorescence properties[9]. There exist different approaches to the implementation of a multispectral imaging system. The optimum system is not clearly defined because its characteristics will be deeply determined by the requirements of the specific intended field of application. Different examples of approaches can be enumerated. One of them is the use of a punctual spectrometer together with a 2D scanning system. It offers high spectral and spatial resolution, but requires high acquisition times to cover the extension of the sample[3]. Another implementation consists of the use of monochrome matrix imaging detectors, CMOS or CCD, conjugated with filter wheels with the intention of generating different spectral channels[5, 10]. This set of elements offers high spatial resolution but due to the sequential movement of the filter wheel, low performances in spectral resolution and time acquisition are achieved. Different additions to this idea have been developed in order to increase the velocity of the system. The use of a lenslet array with different spectral filters between each lens element and the imaging sensor or filter mosaics in front of the sensor surface are options that increases the acquisition rate in expense of spectral and spatial resolution[11, 12]. The inclusion of tunable filters of liquid crystal or acousto optic technology also tries to overcome the problems of the filter wheel devices but instead increases the cost of the system considerably[13].

Another kind of multispectral systems has become attractive with the current development and availability of the LED technology. LED illumination technology is very cheap and efficient, has a long lifecycle and is constantly evolving. These elements have narrow-spectral emission and are available in several wavelengths over the different spectral ranges of the UV, VIS and NIR. They allow illuminating with a wide number of different specific wavelengths or customized combinations of them in a fast way and in a switching synchrony with the imaging sensors. The increased publications in this type of LED systems show that new possibilities are being explored trying to decrease the acquisition time and costs

by employing off-the-shelf elements[14-17]. Following this trend, in this work we show the simulated recovery results for an imaging system using LED illumination assuming realistic noise parameters, constructed with measurements of the real imaging components. In order to calculate the spectral information, the widely spread pseudo-inverse method has been used[10, 18]. The pseudo-inverse technique computes the transform between system responses and reflectance without any a priori knowledge about the imaging system but needs a training process with known spectral reflectances and their respective camera responses.

2. EXPERIMENTAL SETUP

We present the simulations of spectral reconstruction for the following multispectral imaging system. Its experimental setup can be described as having two different modules; the first module consists of a CCD monochrome cooled camera with 12 bit depth and 16 groups of LEDs where each group has a specific central wavelength of emission. They cover the wavelength range from 350nm to 950nm. In a similar fashion, the second module has an InGaAs based camera with 14 bit depth and 7 groups of LEDs with a different central wavelength of emission. This module covers the range of wavelengths from 900nm to 1650nm. Figure 1 shows the measured emission spectra for the LED illumination in the respective module and Table 1 contains the spectral descriptive data for each LED element. In total, there are 23 spectral bands with different wavelength peaks of emission. The measurements of the characteristics of the LEDs were carried out with a commercial scanning spectrometer (model Spectro 320 of Instruments Systems).
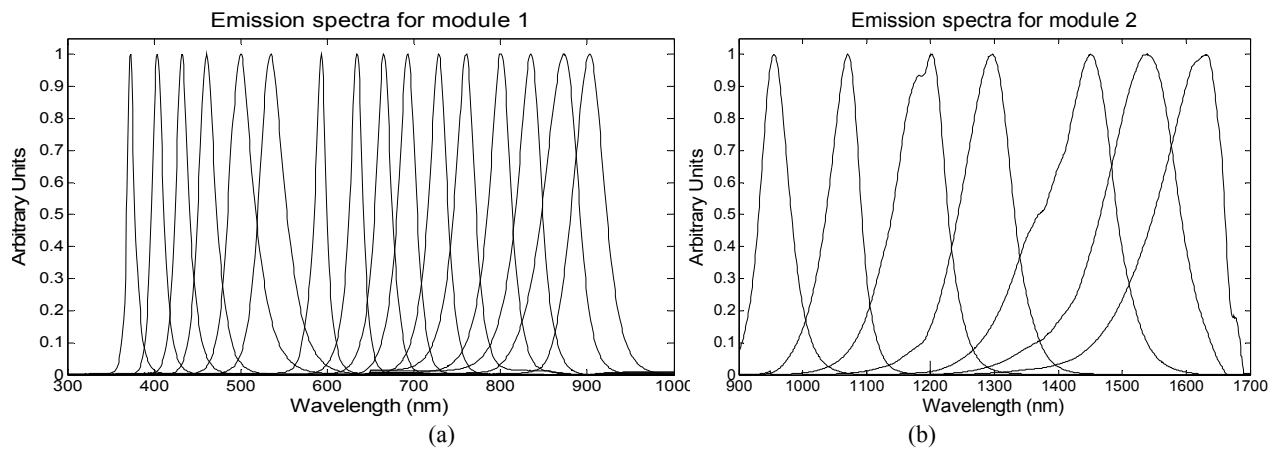

Figure 1. Measured spectra of emission of LED elements. a) emission spectra for the LEDs of the first module and b) emission spectra for the LEDs of the second module.

In our simulations, we used the known reflectance curves of 170 common objects (available from NYU at http://www.cns.nyu.edu/ftp/ltm/SSR/) to be extended and manipulated in order to be employed as the training and measured samples over the ranges of wavelengths that covers the proposed multispectral system.

Table 1. Spectral data for the LED elements comprising the illumination source

Illumination module 1				Illumination module 2	
Peak wavelength (nm)	FWHM (nm)	Peak wavelength (nm)	FWHM (nm)	Peak wavelength (nm)	FWHM (nm)
373	9.5	404	15	955	51
432	17	461	22	1071	53
500	32	535	34	1202	88
593	15	634	16.5	1297	89
665	21	693	23.5	1451	122
728	24	761	26	1540	126
801	28	835	31	1630	111
874	45	903	41		

3. METODOLOGY

3.1 Pseudo-inverse model to recover spectral reflectance

The camera responses, X_i, in arbitrary units of an imaging system when an object with reflectance $R(\lambda)$ is under a specific illumination $I_i(\lambda)$ can be expressed as:

$$X_i = \int_\lambda I_i(\lambda) R(\lambda) S(\lambda)\, d\lambda, \tag{1}$$

where $S(\lambda)$ is the spectral sensitivity of the camera sensor. Assuming a discretely sampled description of the former quantities without considerable loss of information, equation (1) can be re-written in a matrix way as follows:

$$x = C^T r, \tag{2}$$

where r is a reflectance column vector at p sampling wavelengths, x is a q-component column vector of the camera responses, and C is a pxq matrix that contains the product of the spectral sensitivity of the camera and the spectral emission of q different LED illuminations. Therefore, the key question here is to recover the spectral reflectance r of a sample given a vector of camera responses x. In the case of the pseudo-inverse model the solution that it provides is a matrix that operates mapping camera responses to estimated reflectances. This mapping matrix minimizes the least-squares-error for a training set of known reflectances with the correspondent camera responses and does not use prior knowledge of the acquisition system characteristics. If we let be R_t a matrix of m columns of training reflectance samples, and X_t a matrix of m columns of system responses to the training, then the matrix D that takes X_t to R_t is given by:

$$D = R_t X_t^T \left(X_t\, X_t^T \right)^{-1}, \tag{3}$$

where $X_t^T \left(X_t\, X_t^T \right)^{-1}$ is the so called Moore-Penrose pseudo-inverse of the matrix X_t. By applying a matrix D to a system response vector x, i.e., $r = Dx$, a reflectance r is estimated.

3.2 Metrics for spectral evaluation

To evaluate the performance of the system three different metrics are used. Two metrics serve to compare the estimated spectral curves with respect to the original spectra. The root mean square error (RMSE) that is a widely used metric for spectral evaluation[10], and the goodness-of-fit coefficient (GFC) proposed by Hernandez-Andrés *et. al*[19]. This GFC is based on the inequality of Schwartz and it is described by equation (4).

$$GFC = \frac{\left| \sum_j r_o(\lambda_j) r_e(\lambda_j) \right|}{\sqrt{\sum_j [r_o(\lambda_j)]^2 \sum_j [r_e(\lambda_j)]^2}}, \tag{4}$$

where $r_o(\lambda_j)$ is the original spectral data at the wavelength λ_j and $r_e(\lambda_j)$ is the estimated spectrum at the wavelength λ_j. GFC $\geq$ 0.999 and GFC $\geq$ 0.9999 are required for respectively good and excellent matches. The third metric is the CIEDE2000 formula (DE00)[20] used over the reconstructions in the VIS range as a colorimetric evaluation.

4. RESULTS AND DISCUSSION

Results are given for three different conditions: the system under ideal conditions, under the influence of quantization error noise and finally under quantization error and random additive sources of noise. To simulate the quantization, namely, to achieve the simulated digital levels, the equation (5) was used with the *round* function (available in MATLAB software) accounting for the introduction of the quantization error noise.

$$DL_i = round\left(x_i \frac{DL_{max}}{(x_i)_{max}} \right), \tag{5}$$

where DL_i is the digital level for each channel and sample, x_i is the theoretical response of the system, DL_{max} is the maximum digital level corresponding to the bits of the system. In this case there are two different DL_{max} values: 4095 for the first module that uses a 12 bit depth camera and a value of 16383 for the second module that uses a 14 bit depth camera. The *round* function operates providing the nearest integer to the number given as its argument.

To simulate the influence of the additive noise a term was added to the camera responses:

$$x_i' = x_i + n, \tag{6}$$

where x_i' is the camera response influenced by the additive random noise and n is the proportional term of noise introduced. For the simulations a 2% proportional noise was added.
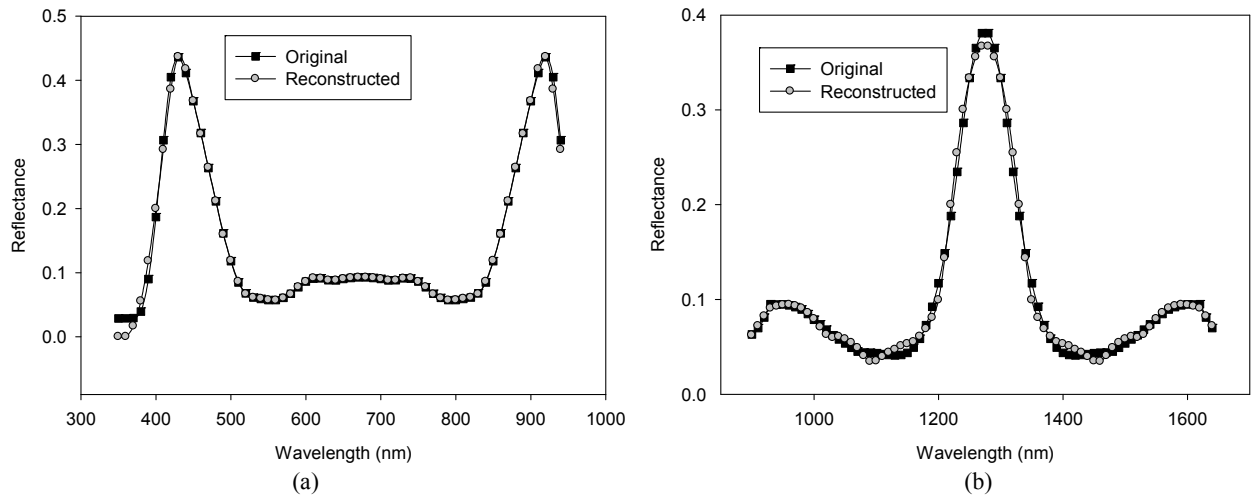

Figure 2. Original and reconstructed reflectances for two samples assuming ideal conditions for the proposed imaging system. a) Result for the first module in the range from 350-950nm. b) Result for the second module over the range 900-1650nm.
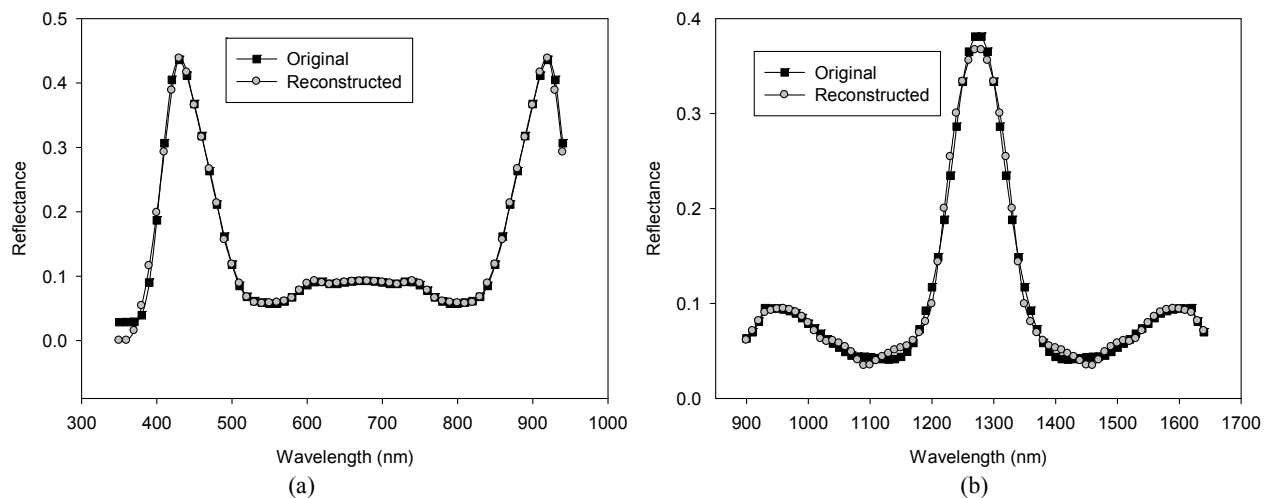

Figure 3. Original and reconstructed reflectances for two samples under quantization error noise. a) Result for the first module in the range from 350-950nm. b) Result for the second module over the range 900-1650nm.
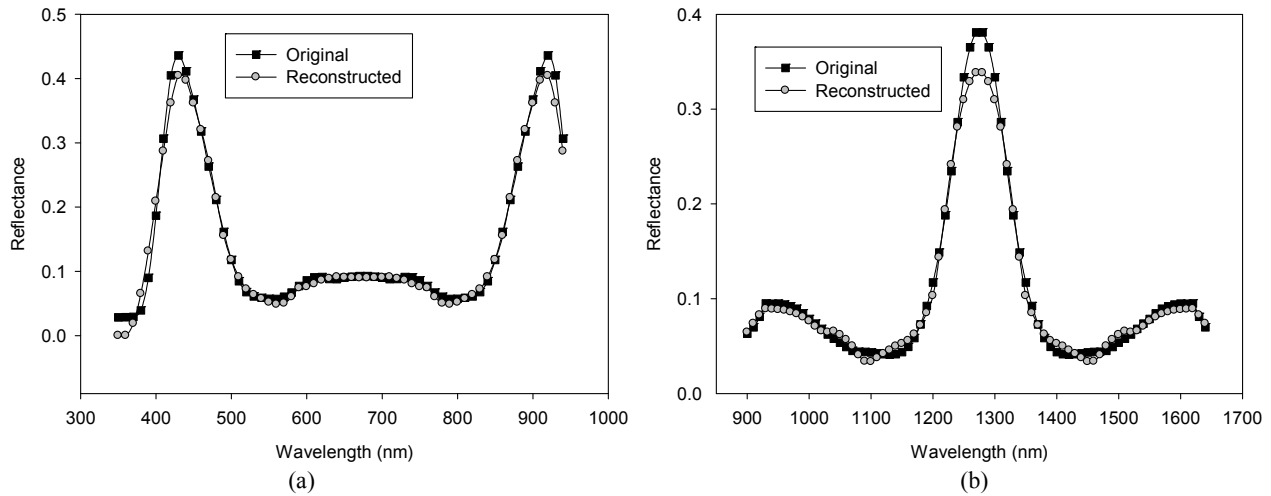
(a) (b)

Figure 4. Original and reconstructed reflectances for two samples under the influence of additive noise and quantization error for the proposed imaging system. a) Result for the first module in the range from 350-950nm. b) Result for the second module over the range 900-1650nm.

Results of reconstructions are shown through Figure 2 to Figure 4, and Table 2 to Table 4. The Figure 2 shows examples of simulated reconstructions of reflectances for ideal conditions in the imaging system. The fitting of the curves is very good. This is also confirmed with the numerical results of the selected metrics for evaluation shown in Table 2. While the module 1 has very accurate reconstructions supported by all the evaluation metrics, module 2 has a good performance but lower evaluation metrics than module 1. This is reasonable given the quantity of different LED illuminations available for each module, 16 for the module 1 and 7 for the module 2. In the Figure 3 and Table 3 the results in term of the evaluation metrics for the reconstruction of the reflectances under the influence of the quantization error are shown. Both modules keep presenting good performance, although the first module has a greater change comparatively to the second module because of the difference in bit depth of the correspondent sensors. Even more, the metrics for the second module are almost unchanged showing a very low influence of the quantization error. In the Figure 4 and Table 4 the reflectance curves of two samples and the evaluation metrics for the complete set of reflectances under the influence of 2% additive noise and quantization error are shown. Although, given the results of the low influence of the quantization error, the differences found in this table with respect to the former ones are attributable mostly to the additive noise. This Table shows again that the second module have less accuracy in the reconstructions something that is expectable given the mentioned difference in number of LED illuminations and spectral width emission of the LED components. Besides of the spectral evaluation, the results in terms of color difference reveal a very good colorimetric performance of the system, only under the influence of additive noise the mean color difference is greater than, but still close to, 1 color difference unit.

Table 2. Results of evaluation metrics assuming ideal conditions in the acquisition system

	Module 1			*Module 2*	
	DE00	RMSE x 100	GFC	RMSE x 100	GFC
Mean	0.0175	0.1684	1.0000	0.9655	0.9991
Min	1.2551e-3	3.7251e-3	0.9991	0.0468	0.9899
Max	0.0986	0.8170	1.0000	4.1661	1.0000

Table 3. Results of evaluation metrics under the influence of the quantization error noise.

	Module 1			Module 2	
	DE00	RMSE x 100	GFC	RMSE x 100	GFC
Mean	0.0863	0.2628	0.9999	0.9687	0.9991
Min	4.3596e-3	0.0697	0.9940	0.0653	0.9899
Max	0.8112	1.3203	1.0000	4.1632	1.0000

Table 4. Results of evaluation metrics under the influence of additive noise and quantization error noise.

	Module 1			Module 2	
	DE00	RMSE x 100	GFC	RMSE x 100	GFC
Mean	1.0169	1.1701	0.9995	2.1150	0.9976
Min	0.2087	0.1122	0.9962	0.1090	0.9790
Max	3.0399	3.1190	0.9999	9.4544	0.9997

5. CONCLUSIONS

In this paper the simulations of reflectance estimation for a multispectral system intended for its future use in the study of artwork are shown. The system that is mainly composed of two modules of acquisition and illumination is evaluated under three different conditions: under ideal conditions for the acquisition, under quantization error noise and finally under the condition of random additive noise. The system performs very accurately for the two modules under ideal conditions. As expected, the first module is more influenced by the quantization process, for the second module the effect is almost negligible. Even so, the results continue to be very good as it is confirmed if the GFC criteria are followed. For the additive noise condition, the performance of the system decays but it is still good, in fact, in terms of the colorimetric evaluation given in the first module, the mean color difference is kept close to 1. Comparatively, the second module has less accuracy than the first module and that fact is closely related to the minor availability of LED elements in the range of wavelengths comprised by this module.

Here we have simulated the performance of a system in development for the study of artwork. The results are given in terms of the measured characteristics of the system components and although, several conclusions can be drawn from this study, they can only be approximations. Therefore, it is the intention of this work to serve as guidance for the final purpose of having the complete operational system.

REFERENCES

[1] Anderson, L. O., Y. E. Shimabukuro, R. S. Defries *et al.*, "Assessment of Deforestation in Near Real Time Over the Brazilian Amazon Using Multitemporal Fraction Images Derived From Terra MODIS," IEEE Geoscience and Remote Sensing Letters 2, 315-318 (2005).
[2] Ariana, D., D. Guyer, and B. Shrestha, "Integrating multispectral reflectance and fluorescence imaging for defect detection on apples," Computers and Electronics in Agriculture 50, 148-161 (2006).
[3] Bonifazzi, C., P. Carcagnì, R. Fontana *et al.*, "A scanning device for VIS–NIR multispectral imaging of paintings," Journal of Optics A: Pure and Applied Optics 10, 064011 (2008).
[4] Sheth, S. A., N. Prakash, M. Guiou *et al.*, "Validation and visualization of two-dimensional optical spectroscopic imaging of cerebral hemodynamics," NeuroImage 47 Suppl 2, T36-43 (2009).
[5] Vilaseca, M., R. Mercadal, J. Pujol *et al.*, "Characterization of the human iris spectral reflectance with a multispectral imaging system," Applied optics 47, 5622-5630 (2008).

[6] Daffara, C., E. Pampaloni, L. Pezzati *et al.*, "Scanning multispectral IR reflectography SMIRR: an advanced tool for art diagnostics," Accounts of chemical research 43, 847-856 (2010).

[7] Karagiannis, G., C. Salpistis, G. Sergiadis *et al.*, "Nondestructive multispectral reflectoscopy between 800 and 1900 nm: An instrument for the investigation of the stratigraphy in paintings," The Review of scientific instruments 78, 065112 (2007).

[8] Tsumura, N., "Appearance reproduction and multispectral imaging," Color Research & Application 31, 270-277 (2006).

[9] Comelli, D., G. Valentini, A. Nevin *et al.*, "A portable UV-fluorescence multispectral imaging system for the analysis of painted surfaces," The Review of scientific instruments 79, 086112 (2008).

[10] Vilaseca, M., J. Pujol, M. Arjona *et al.*, "Multispectral system for reflectance reconstruction in the near-infrared region.," Applied optics 45, 4241-4253 (2006).

[11] Kong, L., D. Yi, S. Sprigle *et al.*, "Single sensor that outputs narrowband multispectral images," Journal of biomedical optics 15, 010502.

[12] Mathews, S., "Design and fabrication of a low-cost, multispectral imaging system," Applied optics 47, F71-76 (2008).

[13] Gat, N., "Imaging spectroscopy using tunable filters: a review," Proceedings of SPIE 4056, 50-64 (2000).

[14] Brydegaard, M., Z. Guan, and S. Svanberg, "Broad-band multispectral microscope for imaging transmission spectroscopy employing an array of light-emitting diodes," American Journal of Physics 77, 104 (2009).

[15] Fauch, L., E. Nippolainen, A. Kamshilin *et al.*, "Optical Implementation of Precise Color Classification Using Computer Controlled Set of Light Emitting Diodes," Optical Review 14, 243-245 (2007).

[16] Fauch, L., E. Nippolainen, V. Teplov *et al.*, "Recovery of reflection spectra in a multispectral imaging system with light emitting diodes," Optics Express 18, 23394 (2010).

[17] Yamamoto, S., N. Tsumura, T. Nakaguchi *et al.*, "Development of a Multi-spectral Scanner using LED Array for Digital Color Proof," Journal of Imaging Science and Technology 51, 61 (2007).

[18] Shen, H.-L., J. H. Xin, and S.-J. Shao, "Improved reflectance reconstruction for multispectral imaging by combining different techniques," Optics Express 15, 5531 (2007).

[19] Hernández-Andrés, J., J. Romero, and R. Lee Jr, "Colorimetric and spectroradiometric characteristics of narrow-field-of-view clear skylight in Granada, Spain," Journal of the Optical Society of America A 18, 412 (2001).

[20] Sharma, G., W. Wu, and E. N. Dalal, "The CIEDE2000 color-difference formula: Implementation notes, supplementary test data, and mathematical observations," Color Research & Application 30, 21-30 (2005).